研究成果報告書

所属機関	職名	氏名
東京理科大学 研究推進機構 総合研究院	研究員(PI)	荒木光典

研究テーマ

大気汚染源となるアルコール類有機化合物に対する
コンパクトな定常監視デバイスの研究開発

1．研究の背景と目的

大気汚染源となるアルコール系揮発性有機化合物の定常監視ができるコンパクトなデバイスの実現を目的とし、キャビティー増幅吸収分光装法を活用する。レーザー光軸調整法を導入して感度の向上を図り、アルコール類の OH 伸縮振動の検出を可能にする。テーブルトップでありながら、アルコール類を他の有機化合物と識別できる技術実証モデルの開発を目指す。

光化学オキシダントに係る大気汚染の状況はいまだ深刻であり、健康被害も数多く報告されている。その最大の原因は、揮発性有機化合物（VOC：Volatile Organic Compounds）である。これら VOC の排出を抑制するためには、定常的な監視すなわち「モニタリング」が必須である。しかし、既存の測定方法の多くは装置内に可動部を持つため、モニタリングに耐えられない。そこで、可動部を持たない測定方法が必要である。キャビティー増幅吸収分光法はその条件を満たしている。２枚の高反射率ミラーからなるキャビティーの中に白色光を入射し多重往復させた後に分光器に導く。そして、ミラー間に導入された VOC を測定する。これまで国内には高分解能型の本装置の開発実績は無かったが、申請者らのチームは可視および近赤外の領域においてその開発に初めて成功した。そして、有機化合物のほとんどが共通に持つ CH 伸縮振動の第 3 倍音（v = 4–0）の検出を達成した。これにより VOC の検出が実証できたため、次の課題として「アルコール類の選択的な検出」を目指している。本研究では、CH 伸縮振動の数分の一の強度しか持たない OH 伸縮振動の検出を目指す。これにより、アルコール類の選択的モニタリングができることを実証する。

2．研究成果および考察

概要

ＯＨ基を持つ VOC である酢酸メチルと酢酸エチルの測定を試みた。しかし、OH 伸縮振動の検出はベースラインとの識別が難しく、今年度は達成できなかった。そこで、CH 伸縮振動の第 4～5 倍音（ν = 5–0～6–0）の吸収スペクトルの探査を行い、その検出に成功した。本研究での高感度化の結果、基音（ν = 1–0）吸収の約 5000 分の 1 の強度をもつ ν = 6–0 への吸収が 400 秒積算において S/N～16 で観測された。さらに、得られた吸収のピークから CH 伸縮振動の分子定数である調和振動数と非調和項を算出できた。よって今後、これら分子の様々な波長帯でのモニタリングが可能になった。

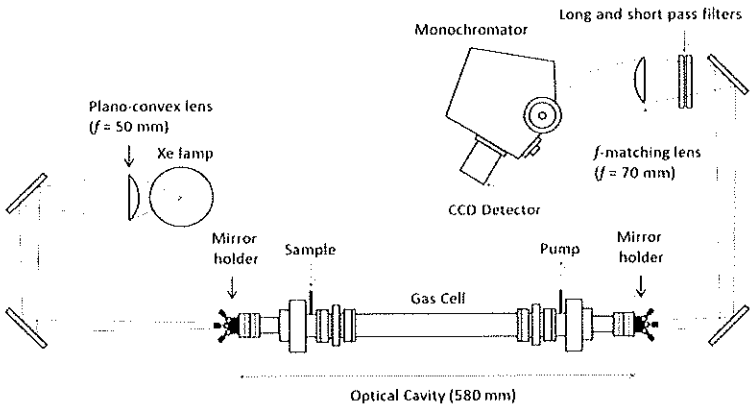

図１、キャビティー増幅吸収分光装置の概念図

開発

キャビティー増幅吸収分光法は、2 枚の高反射率ミラー（反射率 99.99%）の間に白色光を導入してこれを多重往復させることで非常に長い光路長を確保し、高感度の吸収分光を実現する手法である。CCD 検出器を組み合わせることで、広帯域の高速測定が可能となる（図１）。この手法は、測定中に機械的動作を必要としないことから、長期間に渡るモニタリングも可能である。

本研究では、白色光に高安定 Xe ランプの光をレンズで平行光線にして利用した。ここで、ミラーの反射帯域以外の不要な光はキャビティーを素通りして分光器内の迷光になる。それが著しく感度を低下させる。そこで、本年度は特に、高感度化のためロングパスとショートパスのフィルタを各 2－3 枚組み合わせ、ミラーの反射帯域以外の不要な光を除去した。キャビティーから透過したミラー反射帯域の光のみをレンズで集光して分光器に導光した。光学キャビティーから透過した、ミラー反射帯域の光のみをレンズで集光して分光器（HORIBA Jobin/Yvon 製 iHR320）に導光し、グレーティング（刻線数 1200 本/mm）によって分散させて高感度 CCD 検出器（ANDOR 製 iDus 416）によって検出した。

試料セルとして、パイレックス製の円筒セル（内径: 33 mm 長さ: 270 mm）を用い、油回転真空ポンプによって真空引きした。そこに、試料である酢酸メチルまたは酢酸エチル（図 2）を遷移強度に応じて 4－156 Torr 導入した。100－400 秒の積算を行い、スペクトルを得た。波長補正には水銀およびアルゴンの輝線を用いた。

これらの装置は幅 150 cmの実験台に収まるため、テーブルトップの技術実証モデルの開発に成功した。

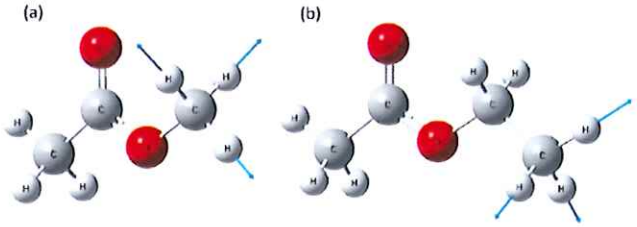

図２、酢酸メチル（a）と酢酸エチル（b）の分子構造とその CH 伸縮振動
本研究における量子化学計算による

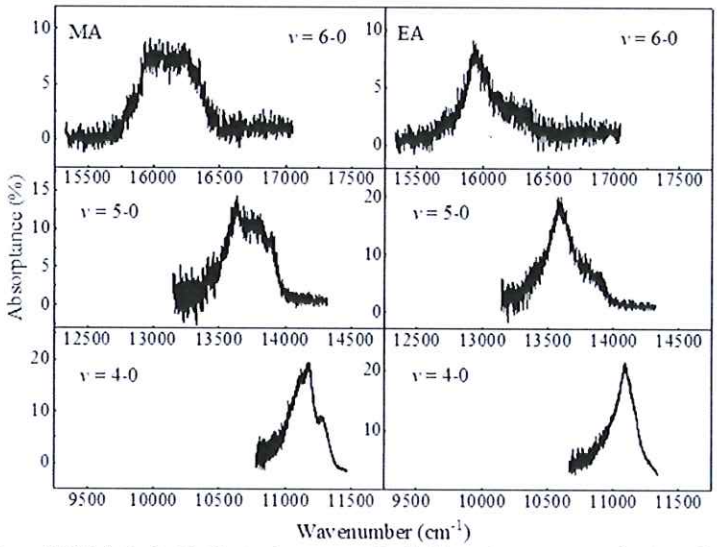

図３、観測された酢酸メチル(MA)と酢酸エチル(EA)の高次倍音

開発と測定の結果

図３に酢酸メチルと酢酸エチルにおける第 3~5 倍音（$\nu = 4-0$ ～ $6-0$）の吸収スペクトルを示す。脂肪族化合物において、CH 伸縮振動の高次倍音の強度は振動量子数が一つ大きくなるにつれて約 9 分の 1 に減少する。ゆえに、特に高感度を必要とした酢酸エチルの測定帯域は 590－650 nm（$\nu = 6-0$ 倍音帯）である。その強度は基音吸収の約 5000 分の 1 である。その測定のために反射帯域 580－665 nm のミラーを用いた。ショートパスとロングパスフィルタを組み合わせて迷光の除去を試みたが、当初の 550－675 nm 帯を透過するフィルタ設定では、スペクトルのピーク構造が得られなかった。そこで、透過帯を 590 – 675 nm 帯に絞ることでピークの検出ができた。すなわち、ミラーの反射帯域の境界領域の光でも強い迷光になる。その 550－590 nm 帯の光を除去することにより感度を 20 倍以上向上することに成功した。よって、400 秒積算において S/N ~ 6 で観測された。このように、本研究で開発した

キャビティー増幅吸収分光装置は、非常に微弱なバンドの観測が可能である。これをもって、技術実証モデルの開発に成功した。そして、これらフィルタの仕様を実用モデルの仕様として提唱できる。

酢酸メチルと酢酸エチルの両化学種において、約 2500 cm^{-1} 間隔の吸収ピークで観測された。酢酸エチルでは第 3~5 倍音のいずれにおいても単一の鋭いピークが観測されたが、酢酸メチルでは大小二つのピークが隣接した構造がみられた。これは酢酸メチルの高次倍音には、非調和項の異なる振動モードが混在しているためだと考えられる。

振動構造はローカルモードモデルを用いて解析した。これは、分子の中で特定の原子対が他の原子とは独立に単独で振動するという高次倍音をうまく説明できる近似である。振動量子数を v、調和振動数を ω_e、非調和項を $\omega_e x_e$ とすると、エネルギーレベル $G(v)$ は下記の式で表すことができる。

$$G(v) = \omega_e (v + 1/2) - \omega_e x_e (v + 1/2)^2 + \ldots,$$

高次倍音 v'–0 の振動数を $\Delta G(v')$ とすると $\Delta G(v') = (\omega_e - \omega_e x_e) v' - \omega_e x_e v'^2$ となる。本研究では、CH 伸縮振動の調和振動数と非調和項を表 1 のように決定した。これらにより、赤外から可視にかけて複数存在する倍音の振動数を求めることができる。よって、酢酸メチルと酢酸エチルの様々な波長帯でのモニタリングが可能になった。（詳細は原著論文 1 参照）

表 1、酢酸メチルと酢酸エチルの CH 伸縮振動の調和振動数 ω_e と非調和項 $\omega_e x_e$ (cm^{-1})

	ω_e	$\omega_e x_e$
酢酸メチル	3083.5(18)	60.0(6)
酢酸エチル	3088.6(40)	61.9(9)

カッコ内は 1σ の誤差を示す。

この他に、本研究の試行錯誤の波及効果として、ヨウ化シアンイオン ICN^+をキャビティーリングダウン分光装置にて測定することに成功した。得られたスペクトルの解析の結果、この分子の電子遷移の持つ固有の吸収波長を精密に決定することができた。（原著論文 2）

3．将来展望

2021 年度の開発において、本装置により CH 伸縮振動の高次倍音の検出が可能であることが示された。しかし、NH や OH 高次倍音についての検証はまだできていない。これらの高次倍音を検出することで、VOC の検出が広く行うことができるようになる。今後はこれらの高次倍音の検出を行う。

4．研究発表

原著論文

1. Mitsunori Araki, Takeru Sato, Takahiro Oyama, Shoma Hoshino, Koichi Tsukiyama, "Gas-phase CH-Overtone band spectra of methyl acetate and ethyl acetate via incoherent broad-band cavity-enhanced absorption spectroscopy," *Chemical Physics Letters*, **796**, 139568 (2022), https://doi.org/10.1016/j.cplett.2022.139568 謝辞記載（添付）
2. Mitsunori Araki, Takumi Ito, Shoma Hoshino, Koichi Tsukiyama, "Rotationally resolved gas-phase spectrum of the A–X electronic transition for the cyanogen halide radical cation ICN^+," Journal of Molecular Spectroscopy 111675-111675 (2022), https://doi.org/10.1016/j.jms.2022.111675 謝辞記載（添付）
3. Mitsunori Araki and Ken Matsuyama, "Rapid Measurements of Hydrogen Cyanide Concentration in Combustion Gas via Terahertz Spectroscopy," *Current Applied Physics*, **36**, 83-87, (2022), https://doi.org/10.1016/j.cap.2021.12.015

著書

1. 日本分光学会 監修、紫外可視・蛍光分光法、講談社、築山光一、星野翔麻、5.1 キャビティーリングダウン分光法： 微量成分検出への応用 （10 頁）分担執筆、2021 年 8 月 27 日、 ISBN: 978-4-06-523805-9

研究会主催

1. キャビティーリングダウン分光ユーザーズミーティング、zoom 開催、2021 年 12 月 17 日、https://www.rs.kagu.tus.ac.jp/tsukilab/crds_um/

国際会議

1. "LABORATORY SPECTROSCOPY OF $A^2\Sigma^+$–$X^2\Pi_{3/2}$ ELECTRONIC TRANSITION OF ICN^+ TO

ESTIMATE PROFILES OF INTERSTELLAR ABSORPTION LINES BY HALOGEN CYANIDE CATIONS," TAKUMI ITO, MITSUNORI ARAKI, et al., International Symposium on Molecular Spectroscopy, Champaign-Urbana, Illinois (US), (2022, 6, 20-24)

2. "GAS-PHASE CH-OVERTONE BAND SPECTRA OF METHYL ACETATE AND ETHYL ACETATE VIA INCOHERENT BROAD-BAND CAVITY-ENHANCED ABSORPTION SPECTROSCOPY," TAKERU SATO, MITSUNORI ARAKI, et al., International Symposium on Molecular Spectroscopy, Champaign-Urbana, Illinois (US), (2022. 6. 20-24)
3. "Development of cavity enhanced absorption spectrometer and detection of CH overtones of methyl acetete and ethyl acetete," Mitsunori Araki, et al., The Users Meeting of Cavity Ringdown Spectroscopy, (2021.12.17)

Chemical Physics Letters 796 (2022) 139568

Contents lists available at ScienceDirect

Chemical Physics Letters

journal homepage: www.elsevier.com/locate/cplett

Gas-phase CH-Overtone band spectra of methyl acetate and ethyl acetate via incoherent broad-band cavity-enhanced absorption spectroscopy

Mitsunori Araki [a,b,*], Takeru Sato [a], Takahiro Oyama [a], Shoma Hoshino [a], Koichi Tsukiyama [a]

[a] Department of Chemistry, Faculty of Science Division I, Tokyo University of Science, 1-3 Kagurazaka, Shinjuku-ku, Tokyo 162-8601, Japan
[b] Research Institute of Science & Technology, Tokyo University of Science, 2641 Yamazaki, Noda, Chiba 278-8510, Japan

ARTICLE INFO

Keywords:
Cavity
CH-stretching
Overtone
Methyl acetate
Ethyl acetate

ABSTRACT

Gas-phase overtone bands of methyl acetate and ethyl acetate were detected for up to $\nu = 6$–0 by incoherent broad-band cavity-enhanced absorption spectroscopy. The signal-to-noise ratios of $\nu = 4$–0 were achieved to be 40–50 by the 100 s integration time, suggesting an application possibility of this spectroscopic technique for environmental monitoring. Profiles of the observed overtone bands were analyzed in detail with the aid of theoretical calculations and their remarkable peaks were assigned to the progressions starting from the symmetric CH-stretching bands. The harmonic frequencies, the anharmonicities, and the dissociation energies were derived.

1. Introduction

The atmospheric degradation of volatile organic compounds (VOCs) has been of great interest because of their contribution to the chemical network on the earth. Ester taking the form of RCO_2R', where R and R′ are the hydrocarbon parts, is one of the most important classes of VOCs. Ester exists in space as methyl formate [1], methyl acetate [2], and others. On the earth, though natural source of ester is fruits, it is known that industrial activities are responsible for the release of ester to atmosphere [3]. For instance, ester is frequently used as paints, adhesion bonds, fumigants, perfume, and organic solvents. Thus, it is crucial to understand about basic spectroscopic features including vibrational structure of ester to carry out quantitative monitoring in indoor and outdoor environments.

The CH-stretching overtone bands could be excellent probes for environmental monitoring, as their spectroscopic frequencies fall in the "atmospheric windows" and have less overlapping with vibrational peaks of inorganic gases. Profiles of the overtone bands are useful identifiers of molecular species, as overtone bands generally consist of superimpose of a number of vibrational modes. Thus, prior to monitoring, spectroscopic measurements of profiles for individual ester compounds in laboratory are essential.

Environmental monitoring of chemical species requires us to measure gas concentrations and compositions over a long period of time. Fourier transform infrared (FT-IR) spectroscopy, for example, is employed as a commonly used reliable way to evaluate gas concentrations. This spectroscopic method measures absorption lines belonging to vibrational transitions. However, this spectroscopic technique is not preferable for long-period continuous monitoring, because a mechanical moving part (mirror) is indispensable for acquiring an interference pattern.

Incoherent broad-band cavity-enhanced absorption spectroscopy (IBB-CEAS, hear after CEAS) developed by Fiedler et al. [4] seems to be ideal for long-period monitoring, because no moving parts are required during measurement. The apparatus for this spectroscopic method generally consists from a continuous light source, an optical cavity, and a spectrometer. Thus, frequent replacements of mechanically moving components are not necessary. CEAS has been evaluated for detections of the electronic transitions of gas-phase molecules [567] and the particle scattering by aerosols [8]. However, this relatively new spectroscopic approach has not been tested for detections of overtone bands so far.

Methyl acetate (MA) and Ethyl acetate (EA) are simple and fundamental esters. The vibronic structure of fundamental bands in the infrared region up to 3050 cm^{-1} for EA in liquid and crystalline states was observed by Mido et al. [9]. The vibrational feature up to 4000 cm^{-1} for MA was investigated in solid Argon by Patten et al. [10]. Overtone bands of MA and EA in the liquid phase were observed as wide-range lower-resolution spectra [11]. On the other hand, for the practical monitoring of VOCs in environment, it is essential to understand spectral

* Corresponding author.
E-mail address: araki@rs.tus.ac.jp (M. Araki).

https://doi.org/10.1016/j.cplett.2022.139568
Received 5 February 2022; Accepted 14 March 2022
Available online 16 March 2022

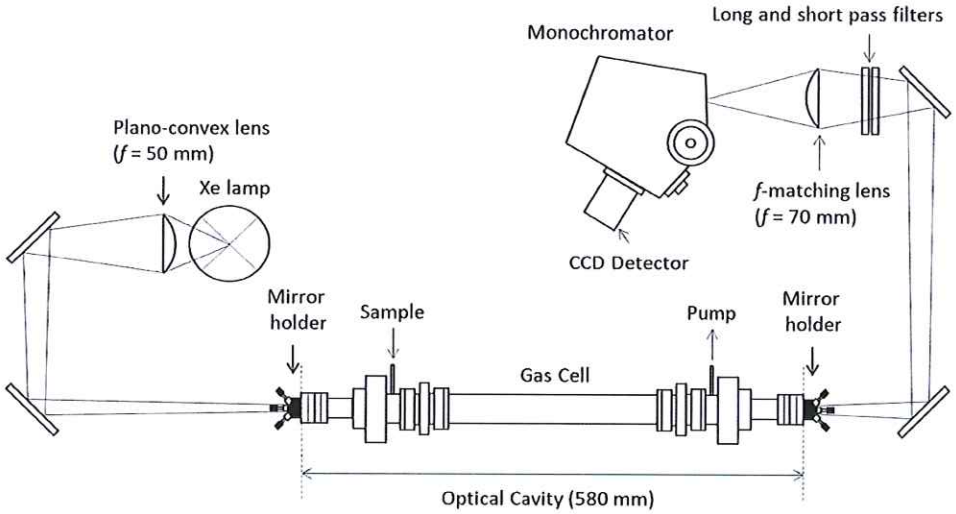

Fig. 1. Setup of incoherent broad-band cavity-enhanced absorption spectrometer.

profiles of corresponding compounds in the gas phase, which would differ considerably from those in the condense phase. The vibrational structure was reported for EA in the gas phase up to 1900 cm^{-1} by Ha et al. [12]. However, overtone bands for both MA and EA in the gas phase, which are expected to appear in the visible and near-infrared range, have not been recorded for far.

In this paper, we report construction of a totally new apparatus for CEAS and its sensitivity evaluation by measuring VOC's overtone bands of MA and EA. The gas-phase profiles of the $v = 4$–0, 5–0, and 6–0 CH-stretching overtone bands were presented for the first time. Finally, we discuss their spectroscopic parameters as identifiers to monitor VOCs.

2. Experimental

A setup of incoherent broad-band cavity-enhanced absorption spectrometer was newly constructed, as shown in Fig. 1 [13]. As a continuous light source, a Xe-lamp (Hamamatsu L2173) was used in the case of observations in a 586–761 nm range and a tungsten lamp was utilized in the case of 871–937 nm to prevent disturbance by strong atomic emission lines of Xe. Light output from the Xe (tungsten) lamp was roughly parallelized and slightly converged by using a plano-convex lens of $f =$ 50 mm. The pair of the dielectric multi-layer mirrors having a reflectance of $R \sim 0.9999$ over a wavelength range of roughly 100 nm and a diameter of 0.8–1.0 in. was installed to construct an optical cavity as windows of a gas cell by using a pair of mirror holders (CRD optics, 902–8008). After passing through short-pass and long-pass filters, light output from the cavity was focused on an inlet of a monochromator (HORIBA Jobin Yvon iHR320) by using an f-matching plano-convex lens of $f = 70$ mm. The monochromator having a focal length of 320 mm used a grating with groove density of 1200 grooves/mm, giving a resolution of 0.03 nm per pixel at maximum. We applied a slit width of 0.1 mm, which provides an effective full width at half maximum (FWHM) resolution of 2 cm^{-1}. The dispersed emission was detected by a CCD detector (ANDO, iDUS416, 2000 × 256 pixels) cooled at − 70 °C. This can cover a wavelength range of ~ 60 nm (~1100 cm^{-1} at around 730 nm), which allows us to record a whole profile of each overtone peak. Integration time was 100 s for $v = 4$–0, 200 s for $v = 5$–0, and 400 s for $v = 6$–0. Obtained spectra were calibrated in an accuracy of 0.4 cm^{-1} by atomic lines from a mercury lamp.

The short-pass and long-pass filters were used to cut background light out of a reflection band of the dielectric multi-layer mirrors. This process is extremely important practically, because the light output from the Xe (tungsten) lamp can enter almost directly to the monochromator without these filters. A light intensity in the background light would be ~ 10^4 times stronger in unit wavelength than that in the reflection band, causing strong stray light in the monochromator. The combinations of the filters and the reflection bands of the mirrors are listed in Table 1.

Table 1
Cut-on and cut-off wavelengths of long-pass and short-pass filters (nm).

Reflection band of mirror[a]	Observed wavelength range	Transition	Cut-on	Cut-off
580–665	586–652	$v = 6$–0	520, 550, 590	675, 800
700–820	698–761	$v = 5$–0	695	750, 800
825–935	871–937	$v = 4$–0	650, 850	1000

[a] approximately.

To measure the $v = 4$–0 overtone bands of MA and EA, individual samples were filled in the gas cell at a pressure of 2–6 torr. However, to detect the higher overtone bands of $v = 5$–0 and 6–0, their pressures were set at 10–20 torr because of their weaker intensities. The pressure inside the gas cell was measured by a thermocouple vacuum gauge. All the measurements were performed at room temperature (294 K).

A Fourier transform infrared (FT-IR) spectrometer (JASCO, FTIR-4600) was used to record infrared spectra of the $v = 1$–0 fundamental bands and the $v = 2$–0 first overtone bands, where the resolution was set at 1.0 cm^{-1}. A 150-mm gas cell having quartz windows allowing transparency of over 2000 cm^{-1} was installed in the spectrometer. Each sample gas was filled at the pressure of ~ 20 torr after evacuation. The scan speed was set at 2 mm/sec, and the integration was repeated 200 times.

To assign observed peak structures of the $v = 1$–0 fundamental bands, we calculated the vibronic structures of MA and EA by CAM-B3LYP/6–311 + G(d,p) using the program package Gaussian 09 W [14], as shown in Fig. 2. Anharmonic frequencies were evaluated by the function of "anharmonic," as listed in Table 2.

3. Results and discussion

3.1. Detection of overtone bands

The CH-stretching overtone bands of $v = 4$–0, 5–0, and 6–0 in gas phase were detected by CEAS as described in Fig. 3. The $v = 4$–0 band would be suitable for practical use in monitoring, because this band is the strongest in the CCD wavelength range (400–1000 nm). For this band, we achieved signal-to-noise ratios of 40–50 in the 2000-ch spectra

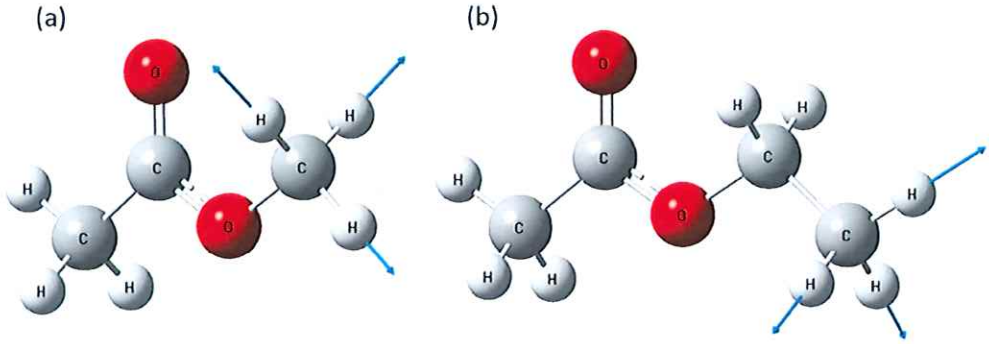

Fig. 2. Examples of symmetric CH-stretching vibrational modes of methyl acetate and trans ethyl acetate. (a) 2963 cm^{-1}, (b) 2928 cm^{-1}.

Table 2
Calculated and observed vibrational frequencies of CH-stretching modes for methyl acetate and ethyl acetate in gas phase (cm^{-1}).

Transition	methyl acetate			ethyl acetate		
v	Calculated [a]	Assignment [b]	Observed [c]	Calculated [a]	Assignment [b]	Observed [c]
7–0			18226(36) [d]			18153(58) [d]
6–0	---	---	15985(40)	---	---	15938(20)
5–0	---	---	13632(40)	---	---	13588(20)
4–0	---	---	11125(40)	---	---	11083(20)
3–0	---	---	8531(9) [d]	---	---	8522(16) [d]
2–0			5970(10)			5969(10)
			5800(10)			5821(10)
1–0	3042	CH_3 s [e]	3002(5)	3040/3040	CH_3 s [e]	
	3032	CH_3 s [e]		3008/3013	C_3H_6 a	
	3009	CH_2 a		3007/3002	C_3H_6 a	
	3001	CH_2 a		3002/2995	CH_3 s [e]	2995 (2)
	2990	CH_3 s		2974/2986	C_2H_4 a	
	2963	CH_3 s	2964(2)	2981/2972	CH_3 s	
	---	---	---	2966/2967	CH_3 s	2964(2)
	---	---	---	2928/2989	CH_2 s	

[a] Anharmonic frequencies (trans/gauche conformers) by CAM-B3LYP/6–311 + G(d,p) using the program package Gaussian 09 W.
[b] The "s" and "a" show symmetric and anti-symmetric, respectively, in a C_s symmetry for the trans conformer.
[c] Values in parentheses denote the uncertainties of peak positions and apply to the last digit of the values.
[d] Estimated from ω_e and $\omega_e x_e$ in Table 3.
[e] Anti-symmetric in a CH_3 structural unit, though symmetric in a C_s symmetry.

for MA and EA by the 100 s integration time, despite of their total oscillator strengths of $\sim 10^{-8}$ for CH-stretching modes [15,16]. Wide FWHMs (200–300 cm^{-1}) of these bands allow us to use smoothing of spectra, which might raise the detection sensitivity by one order of magnitude. To estimate sensitivity, we assume that there is no contamination by other gases. Additionally, a signal-to-noise ratio of 3 is necessary to detect each gas. Therefore, the detection limit of the current setup of CEAS can be derived to be about 40 millitorr.

3.2. Assignment and analysis of overtone bands

The spectra of the fundamental bands of $v = 1$–0 and the first overtone bands of $v = 2$–0 for MA and EA are illustrated in Fig. 3 with their enlarged version in Fig. 4. The obtained band profiles of $v = 1$–0 to 6–0 can be used as identifiers to monitor both VOCs, because these profiles are individually unique for each compound. To estimate the frequencies of the $v = 3$–0 bands, which cannot be covered by the present spectrometers, and the higher overtone bands such as $v = 7$–0 and over, the observed spectra were analyzed as follows.

A model of local mode, which uses a local anharmonic bond potential function, has been applied to interpret higher-overtone bands for stretching of single bonds, while that of normal mode has been utilized to analyze lower-overtone and fundamental bands. Local mode usually provides non-negligible oscillator strengths of overtone bands. The energy levels of a local mode are fit by the one-dimensional anharmonic oscillator equation.

$$G(v) = \omega_e\left(v+\frac{1}{2}\right) - \omega_e x_e\left(v+\frac{1}{2}\right)^2 + \cdots \quad (1)$$

where $G(v)$ is the energy in wavenumber corresponding to the vibrational quantum number v, ω_e the harmonic frequency, and $\omega_e x_e$ the anharmonicity. The peak frequencies of the v' –0 overtone bands provide ω_e and $\omega_e x_e$ via the following relation with neglect of higher-order terms.

$$\Delta G(v') = (\omega_e - \omega_e x_e)v' - \omega_e x_e v'^2 \quad (2)$$

For MA, the calculated anharmonic frequencies and intensities of the

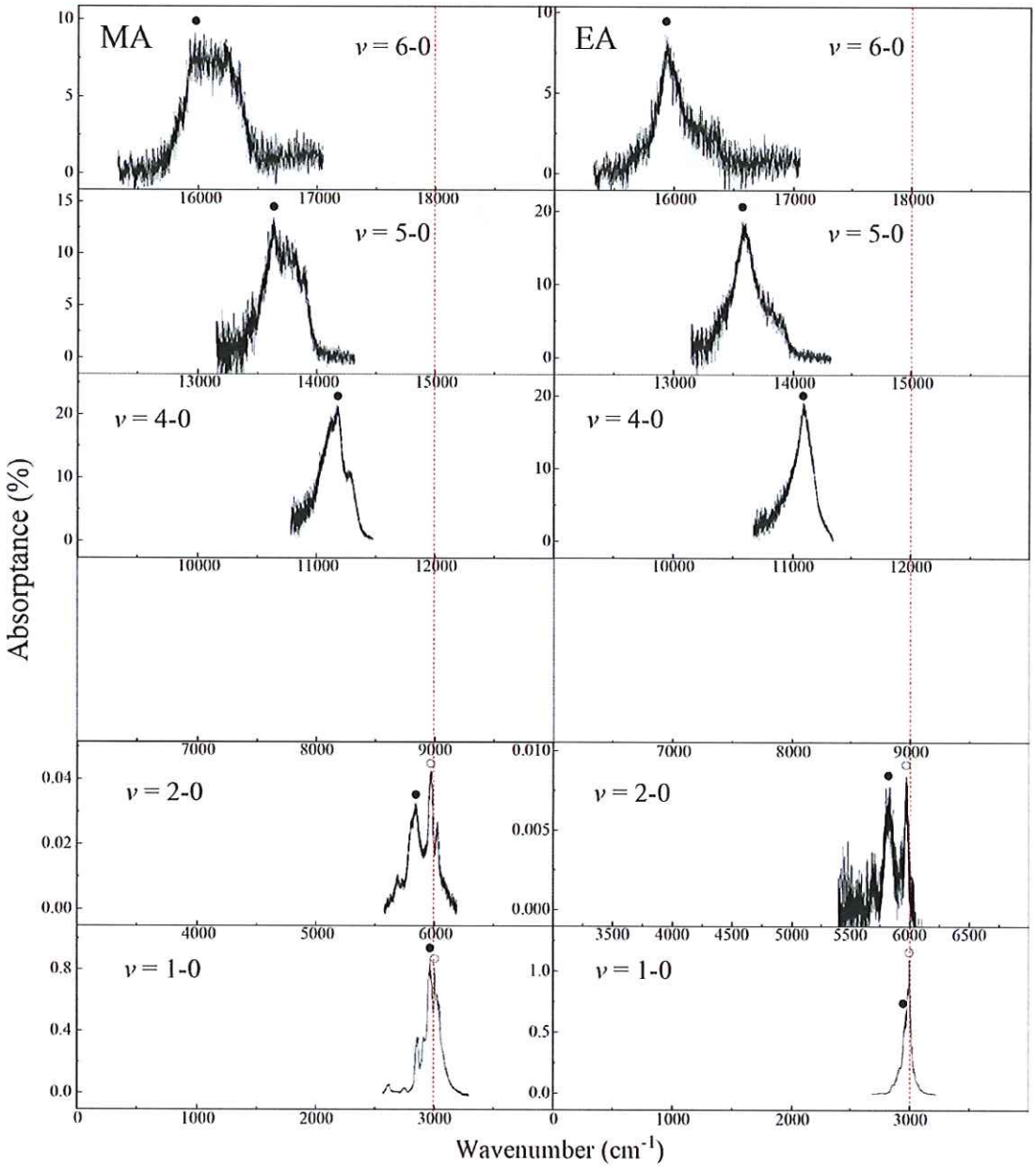

Fig. 3. Observed fundamental and overtone bands for methyl acetate (MA) and ethyl acetate (EA). The lower frequency peaks assigned to the progressions starting from the bundles of the symmetric CH-stretching bands are marked with "●" and the higher-frequency peaks corresponding to the anti-symmetric modes are labeled with "o".

six CH-stretching modes for $\nu = 1$–0 are described as sticks in Fig. 4. The two symmetric CH-stretching modes (solid sticks) in $-CH_3$ structural units produce the bands at relatively lower frequencies, and the four anti-symmetric CH-stretching modes (dotted sticks) show the bands at relatively higher frequencies. Hence, we assumed that the observed lower-frequency peak (marked with "●") in the $\nu = 1$–0 spectrum is assigned to be a bundle of the symmetric CH-stretching bands and the higher-frequency peak (marked with "o") might be that of the anti-symmetric CH-stretching bands. According to the analogy from the assignment of $\nu = 1$–0, we assumed the same assignment for the two peaks of $\nu = 2$–0. The broad profiles appear in the spectra of $\nu = 5$–0 and 6–0 (Fig. 3). We selected the lower-frequency peaks (●) with the stronger intensities in their profiles as main peaks. Generally, a vibrational mode having a larger anharmonicity forms a lower-frequency peak in each overtone profile. Then, the mode with a larger anharmonicity was systematically selected. Hence, the lower-frequency peaks can be assumed as the same series of the "●" marked peaks of $\nu = 1$–0, 2–0, and 4–0. Based on these assumptions, it is reasonable to assign the lower-frequency peaks of $\nu = 4$–0, 5–0, and 6–0 to the progression starting from the bundle of the symmetric CH-stretching bands.

EA has two conformers, the trans conformer that has C_s symmetry with all heavy atoms (O and C) being located within the mirror plane and the gauche conformer with C_1 symmetry [17]. Each conformer has the eight CH-stretching modes [12,17], i.e., the three symmetric CH-stretching modes in $-CH_3$ structural units and the five anti-symmetric CH-stretching modes, as listed in Table 2. The calculated data of the $\nu = 1$–0 band are also described as sticks in Fig. 4, where the symmetric and anti-symmetric modes are represented in solid and dotted sticks,

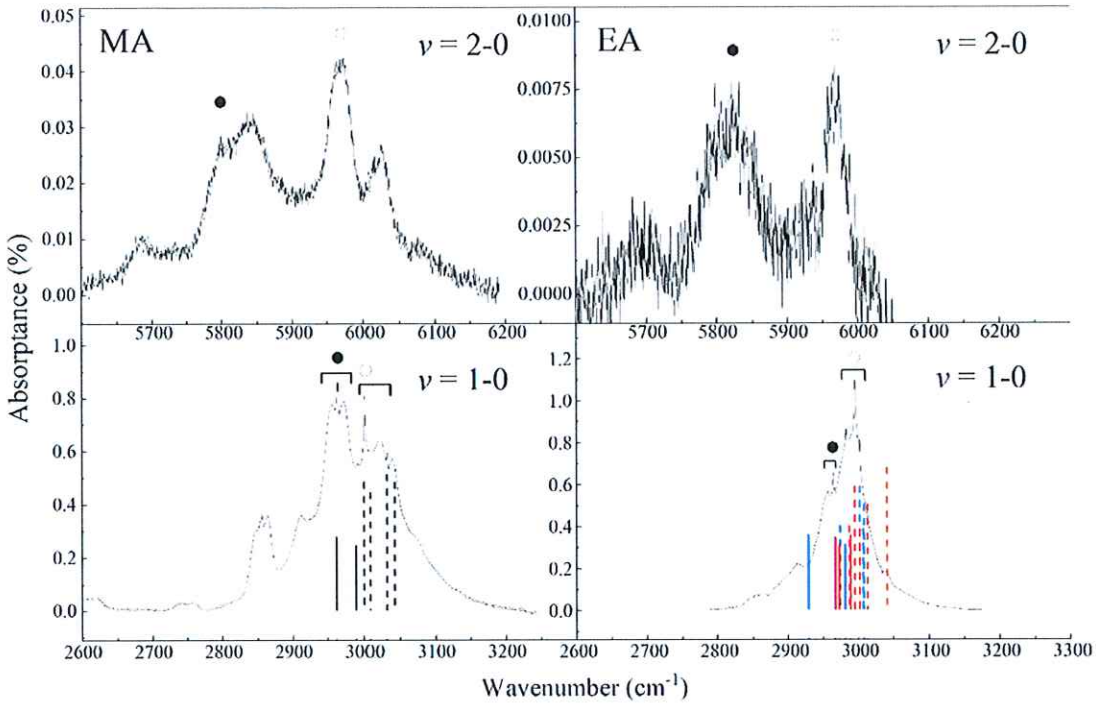

Fig. 4. Observed $\nu = 1$–0 and 2–0 bands comparing with calculated frequencies for methyl acetate (MA) and ethyl acetate (EA). The solid and dotted sticks for $\nu = 1$–0 show the symmetric and anti-symmetric CH-stretching modes, respectively. For EA, the blue and red ticks correspond with the trans and gauche conformers, respectively. The heights of the sticks correspond to the calculated intensities assuming an equivalent amount of the two conformers.

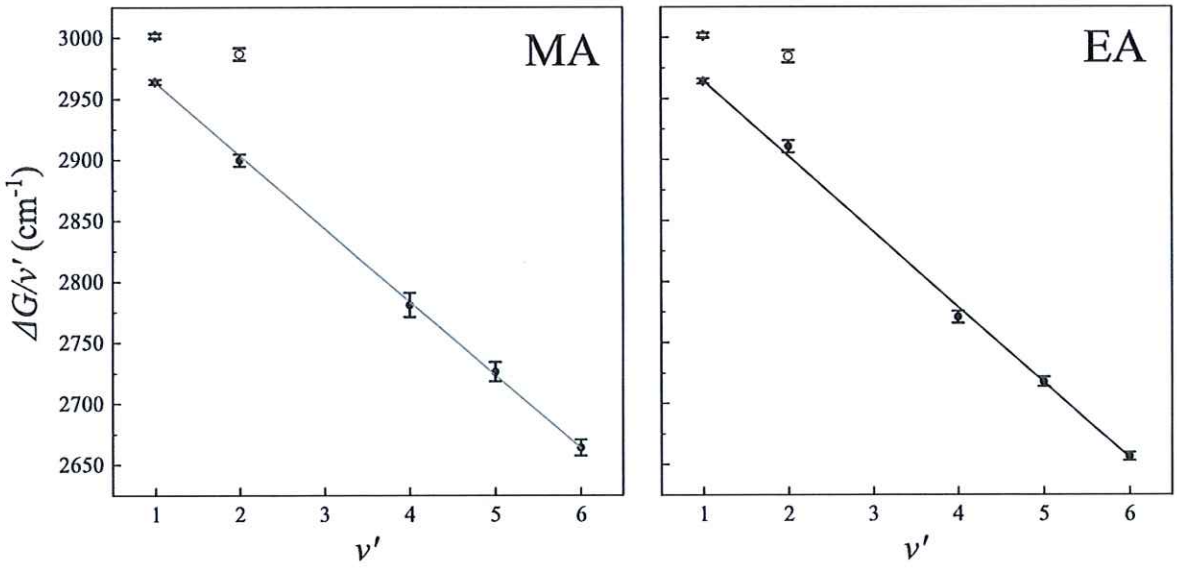

Fig. 5. Birge-Sponer plots of CH-stretching peaks for methyl acetate (MA) and ethyl acetate (EA). These plots are obtained based on Eq. (2).

respectively, and the trans and gauche conformers are in blue and red, respectively. The heights of the sticks show the calculated intensities assuming an equivalent amount of the two conformers. For the $\nu = 1$–0 band, the symmetric modes are located at lower wavelengths than the anti-symmetric modes regardless of the conformer. Thus, it is consistent to assign (●) and (○) to the symmetric and anti-symmetric modes, respectively. The same consideration leads to the tentative assignment for the two peaks of $\nu = 2$–0 as shown in upper panels in Fig. 4. Based on these assumptions, the peaks of $\nu = 4$–0, 5–0, and 6–0 can be expected as the progression starting from a bundle of the symmetric CH-stretching bands.

Our assignment would be justified by Birge-Sponer plots showing in Fig. 5. For both MA and EA, according to Eq. (2), the peaks of $\nu = 4$–0, 5–0, and 6–0 can be consistently explained together with the lower-frequency peaks (●) of $\nu = 1$–0 and 2–0. The lower-frequency peaks are put on straight lines, although the higher-frequency peaks (○) of $\nu = 1$–0 and 2–0 are not on lines. Hence, the peaks of the higher overtone bands can be considered to consist of the series from the symmetric CH-stretching modes for CH_3 and/or CH_2. This is consistent with a fact that the CH-stretching cannot make dissociable anharmonic potentials due to

Table 3
Harmonic frequencies and anharmonicities of CH-stretching for methyl acetate and ethyl acetate (cm^{-1}).[a]

	ω_e	$\omega_e x_e$
methyl acetate	3083.5(18)	60.0(6)
ethyl acetate	3088.6(40)	61.9(9)

[a] Values in parentheses denote the uncertainties (1σ) of fitting and apply to the last digit of the values.

core-core repulsion between C and H atoms [18].

Based on the above assignments, the harmonic frequencies ω_e and the anharmonicities $\omega_e x_e$ of MA and EA were derived as listed in Table 3. By these parameters, the dissociation energies D_0 ($\approx \omega_e{}^2/4\omega_e x_e - G(0)$) from the $v = 0$ level are derived to be 38100 ± 400 and 37000 ± 580 cm^{-1}, respectively, for CH stretching. These energies suggest that overtone bands higher than $v = 6$–0 are observable as additional identifiers of these gases in environment. The frequencies of the $v = 3$–0 and 7–0 overtone bands are estimated by using ω_e and $\omega_e x_e$, as listed in Table 2.

The lower- and higher-frequency peaks of $v = 2$–0 for MA and EA are well separated compared with those of $v = 1$–0, as shown in Figs. 3 and 4. This is because the higher-frequency peaks belong to the anti-symmetric CH-stretching modes having a small $\omega_e x_e$ less than 20 cm^{-1}, while this parameter of the symmetric CH-stretching modes is about 60 cm^{-1} (Table 3). The separation between both the peaks increases according to the vibrational quantum number.

4. Summary

The atmospheric degradation of volatile organic compounds (VOCs) has been greatly interested in the field of environmental science. The CH-stretching overtone bands could be excellent probes for environmental monitoring. Profiles of individual overtone bands, which are specific characteristics of molecular species, are useful as identifiers of VOCs.

The gas-phase CH-stretching overtone bands of $v = 4$–0, 5–0, and 6–0 for methyl acetate and ethyl acetate were detected for the first time in this work by using the incoherent broad-band cavity enhanced absorption spectrometer. The high signal-to-noise ratios of the spectra for both compounds suggest that this spectroscopic method would be applicable to monitoring. The pure-absorption profiles of these bands were measured as identifiers of these compounds. Based on the local-mode analysis, these bands were assigned to be the progression starting from the bundles of the symmetric CH-stretching bands starting at 2964 cm^{-1}. The harmonic frequencies and anharmonicities were determined, and the dissociation energies were derived. The peak wavenumbers of $v = 6$–0 and 7–0, which may serve as potential identifiers, are estimated from these spectroscopic parameters. Hence, monitoring of these compounds might be widely possible in the optical and near-infrared region by using a sensitive CEAS setup.

CRediT authorship contribution statement

Mitsunori Araki: Conceptualization, Validation, Resources, Writing – original draft, Supervision, Project administration, Funding acquisition. **Takeru Sato:** Formal analysis, Investigation, Data curation, Visualization. **Takahiro Oyama:** Methodology. **Shoma Hoshino:** Writing – review & editing. **Koichi Tsukiyama:** Writing – review & editing, Supervision.

Declaration of Competing Interest

The authors declare that they have no known competing financial interests or personal relationships that could have appeared to influence the work reported in this paper.

Acknowledgments

M.A. thanks Grant-in-Aid for Scientific Research (C) (Grant No. 18 K05045) and for Challenging Research (Exploratory) (Grant No. 21 K18663), Paloma environmental technology development foundation, Yamada Science Foundation, ESPEC Foundation for Global Environment Research and Technology, Yashima Environment Technology Foundation, and Takahashi Industrial and Economic Research Foundation.

References

[1] R.D. Brown, J.G. Crofts, F.F. Gardner, P.D. Godfrey, B.J. Robinson, J.B. Whiteoak, Discovery of interstellar methyl formate, Astrophys. J. 197 (1975) L29–L31, https://doi.org/10.1086/181769.

[2] B. Tercero, I. Kleiner, J. Cernicharo, H.V.L. Nguyen, A. López, G.M.M. Caro, DISCOVERY OF METHYL ACETATE AND GAUCHE ETHYL FORMATE IN ORION, Astrophys. J. Lett. 770 (2013) L13, https://doi.org/10.1088/2041-8205/770/1/L13.

[3] HaiLin Wang, L. Nie, J. Li, YuFei Wang, G. Wang, JunHui Wang, ZhengPing Hao, Characterization and assessment of volatile organic compounds (VOCs) emissions from typical industries, Chin. Sci. Bull. 58 (7) (2013) 724–730, https://doi.org/10.1007/s11434-012-5345-2.

[4] S.E. Fiedler, A. Hese, A.A. Ruth, Incoherent broad-band cavity-enhanced absorption spectroscopy, Chem. Phys. Lett. 371 (3-4) (2003) 284–294, https://doi.org/10.1016/S0009-2614(03)00263-X.

[5] Y. Nakashima, Y. Kajii, Determination of nitrous acid emission factors from a gasoline vehicle using a chassis dynamometer combined with incoherent broadband cavity-enhanced absorption spectroscopy, Sci. Total Environ. 575 (2017) 287–293, https://doi.org/10.1016/j.scitotenv.2016.10.050.

[6] M. Triki, P. Cermak, G. Méjean, D. Romanini, Cavity-enhanced absorption spectroscopy with a red LED source for NOx trace analysis, Appl. Phys. B. 91 (1) (2008) 195–201, https://doi.org/10.1007/s00340-008-2958-x.

[7] R.A. Washenfelder, A.O. Langford, H. Fuchs, S.S. Brown, Measurement of glyoxal using an incoherent broadband cavity enhanced absorption spectrometer, Atmos. Chem. Phys. 8 (2008) 7779–7793, https://doi.org/10.5194/acp-8-7779-2008.

[8] W. Zhao, M. Dong, W. Chen, X. Gu, C. Hu, X. Gao, W. Huang, W. Zhang, Wavelength-Resolved Optical Extinction Measurements of Aerosols Using Broad-Band Cavity-Enhanced Absorption Spectroscopy over the Spectral Range of 445–480 nm, Anal. Chem. 85 (4) (2013) 2260–2268, https://doi.org/10.1021/ac303174n.

[9] Y. Mido, H. Shiomi, H. Matsuura, M.A. Raso, M.V. Garcia, J. Morcillo, Vibrational spectra, normal vibrations and rotational isomerism of ethyl acetate and three deuterated analogues, J. Mol. Struct. 176 (1988) 253–277, https://doi.org/10.1016/0022-2860(88)80246-1.

[10] K.O. Patten, L. Andrews, Fourier-transform infrared spectra of HF complexes with acetic acid and methyl acetate in solid argon, J. Phys. Chem. 90 (1986) 1073–1076, https://doi.org/10.1021/j100278a023.

[11] J.W. Ellis, The near infra-red absorption spectra of some aldehydes, ketones, esters and ethers, J. Am. Chem. Soc. 51 (5) (1929) 1384–1394, https://doi.org/10.1021/ja01380a012.

[12] T.-K. Ha, C. Pal, P.N. Ghosh, Ethyl acetate: Gas phase infrared spectra, ab initio calculation of structure and vibrational frequencies and assignment, Spectrochim. Acta Part A Mol. Spectrosc. 48 (8) (1992) 1083–1090, https://doi.org/10.1016/0584-8539(92)80117-F.

[13] M. Araki, T. Oyama, Practical Techniques: Development of Incoherent Broad-Band Cavity Enhanced Absorption Spectrometer, J. Spectrosc. Soc. Japan. 69 (2020) 141.

[14] M.J. Frisch, G.W. Trucks, H.B. Schlegel, G.E. Scuseria, M.A. Robb, J.R. Cheeseman, G. Scalmani, V. Barone, G.A. Petersson, H. Nakatsuji, X. Li, M. Caricato, A. Marenich, J. Bloino, B.G. Janesko, R. Gomperts, B. Mennucci, H.P. Hratchian, J. V. Ortiz, A.F. Izmaylov, J.L. Sonnenberg, D. Williams-Young, F. Ding, F. Lipparini, F. Egidi, J. Goings, B. Peng, A. Petrone, T. Henderson, D. Ranasinghe, V. G. Zakrzewski, J. Gao, N. Rega, G. Zheng, W. Liang, M. Hada, M. Ehara, K. Toyota, R. Fukuda, J. Hasegawa, M. Ishida, T. Nakajima, Y. Honda, O. Kitao, H. Nakai, T. Vreven, K. Throssell, J.A.J. Montgomery, J.E. Peralta, F. Ogliaro, M. Bearpark, J. J. Heyd, E. Brothers, K.N. Kudin, V.N. Staroverov, T. Keith, R. Kobayashi, J. Normand, K. Raghavachari, A. Rendell, J.C. Burant, S.S. Iyengar, J. Tomasi, M. Cossi, J.M. Millam, M. Klene, C. Adamo, R. Cammi, J.W. Ochterski, R.L. Martin, K. Morokuma, O. Farkas, J.B. Foresman, D.J. Fox, Gaussian 09, Revision A.02 (2016). https://gaussian.com/g09citation/.

[15] H.G. Kjaergaard, H. Yu, B.J. Schattka, B.R. Henry, A.W. Tarr, Intensities in local mode overtone spectra: Propane, J. Chem. Phys. 93 (9) (1990) 6239–6248, https://doi.org/10.1063/1.458993.

[16] Z. Rong, D.L. Howard, H.G. Kjaergaard, Effect of the methyl internal rotation barrier height on CH-stretching overtone spectra, J. Phys. Chem. A. 107 (23) (2003) 4607–4611, https://doi.org/10.1021/jp0342879.

[17] M. Sugino, H. Takeuchi, T. Egawa, S. Konaka, Molecular structure and confirmation of ethyl acetate as studied by gas electron diffraction, J. Mol. Struct. 245 (3-4) (1991) 357–368, https://doi.org/10.1016/0022-2860(91)87110-4.

[18] J.M. Hollas, High Resolution Spectroscopy, second ed., Wiley, Chichester, New York, Weinheim, Brisbane, Singapore, Toronto, 1998.

Journal of Molecular Spectroscopy 388 (2022) 111675

Contents lists available at ScienceDirect

Journal of Molecular Spectroscopy

journal homepage: www.elsevier.com/locate/yjmsp

Rotationally resolved gas-phase spectrum of the $\widetilde{A}\ ^2\Sigma^+$–$\widetilde{X}\ ^2\Pi_{3/2}$ electronic transition for the cyanogen halide radical cation ICN^+

Mitsunori Araki [a,b,*], Takumi Ito [a], Shoma Hoshino [a], Koichi Tsukiyama [a]

[a] Department of Chemistry, Faculty of Science Division I, Tokyo University of Science, 1-3 Kagurazaka, Shinjuku-ku, Tokyo 162-8601, Japan
[b] Research Institute of Science Technology, Tokyo University of Science, 2641 Yamazaki, Noda, Chiba 278-8510, Japan

ARTICLE INFO

Keywords:
Absorption
ICN^+
Electronic transition
Rotational constant
$ClCN^+$
Diffuse Interstellar Bands

ABSTRACT

A rotationally resolved gas-phase absorption spectrum of the $\widetilde{A}\ ^2\Sigma^+$–$\widetilde{X}\ ^2\Pi_{3/2}$ electronic transition of the cyanogen iodide radical cation ICN^+ was observed by cavity ring-down spectroscopy for the first time. This cation was produced in a supersonic planar discharge jet through a mixture of ICN in helium. By the aid of *a program for rotational, vibrational and electronic spectra* PGOPHER, the rotational constants were determined to be 0.10700 (12) and 0.11002(12) cm^{-1} for the $\widetilde{A}\ ^2\Sigma^+$ and $\widetilde{X}\ ^2\Pi_{3/2}$ electronic states, respectively, and the band origin to be 18262.083(3) cm^{-1}. The rotational constant ratio β {$= (B'-B'')/B''$} was determined to be −2.8%. The β values for FCN^+, $ClCN^+$, $BrCN^+$, and ICN^+ were also evaluated theoretically by CAM-B3LYP/CEP-121G using Gaussian 09W. The rotational profile of the absorption band and its temperature dependence for $ClCN^+$, one of the important candidates for Diffuse Interstellar Bands, were simulated, aiding us in the identification of this cation as in interstellar space.

1. Introduction

Diffuse interstellar bands (DIBs) are absorption bands of molecules in diffuse clouds appearing in the visible and near-infrared region. Identification of DIB carrier materials is one of the longest-standing unsolved problems in spectroscopy and astrochemistry [1,2] since the first detection of DIBs in 1919 [3,4]. The first identification of DIBs was achieved in 2015 *via* a laboratory work by Campbell et al. [5] in which five DIBs in all were assigned to C_{60}^+ [6,7,8]. Thereafter, no identification has been reported, although further spectroscopic investigation of DIBs is expected to explore the evolution of chemical composition in space.

Feasible candidates of DIBs are neutral radicals and their cations involving linear carbon chains and polycyclic aromatic hydrocarbons because they are supposed to exhibit electronic transitions in the optical and near-infrared region as observed for C_{60}^+. The presence of C_{60}^+ in space infers that molecules can be readily ionized in a diffuse cloud. Additionally, the cyanogen halide radical cations, for instance $ClCN^+$, are also good carrier candidates because both cyanide and halide have been detected widely in space and XCN^+ (X = Cl, Br, and I) shows the $\widetilde{A}\ ^2\Sigma^+$–$\widetilde{X}\ ^2\Pi_{3/2}$ transition in the optical and near-infrared region [9].

Structures of the ground as well as the first excited states of lighter cyanogen cations, FCN^+ and $ClCN^+$, were estimated through the He I photoelectron spectra from the neutral ground state to the cationic states by Franck-Condon (FC) simulations [10]. For heavier species, ICN^+, much information has been accumulated in spite of the difficulty generating a sufficiently large number of cations required for laboratory spectroscopy. Photoelectron spectra of ICN giving information of ICN^+ were reported by Hollas and Sutherley [11], Kovač [12], and Eland et al. [13]. Emission spectra corresponding to the $\widetilde{A}\ ^2\Sigma^+$–$\widetilde{X}\ ^2\Pi_{3/2}$ and $\widetilde{B}\ ^2\Pi_{3/2}$–$\widetilde{X}\ ^2\Pi_{3/2}$ transitions for ICN^+ were detected by Allen and Maier [14], Fulara et al. [9], and Tsuji et al. [15]. Absorption spectra were observed in Ne matrix by Leutwyler et al. [16]. Especially, Fulara and coworkers precisely determined the gas-phase transition energy of the $\widetilde{A}\ ^2\Sigma^+$–$\widetilde{X}\ ^2\Pi_{3/2}$ transition in the accuracy of ±1 cm^{-1} through their spectra were not fully rotationally resolved [9].

Experimental studies covering the three species of XCN^+ (X = Cl, Br, and I) were reported by Fulara et al. [9], Hollas and Sutherley [11], and Chau et al. [17]. These reports suggest that the spectroscopic parameters, such as electronic transition energies and molecular structures, for the cyanogen halide radical cations systematically vary according to the size of the halogen atom. Hence, when one spectroscopic parameter for any one of those cations is experimentally measured, the corresponding

Abbreviations: DIB, Diffuse interstellar band.

* Corresponding author.
E-mail address: araki@rs.tus.ac.jp (M. Araki).

https://doi.org/10.1016/j.jms.2022.111675
Received 21 April 2022; Received in revised form 12 June 2022; Accepted 12 July 2022
Available online 16 July 2022

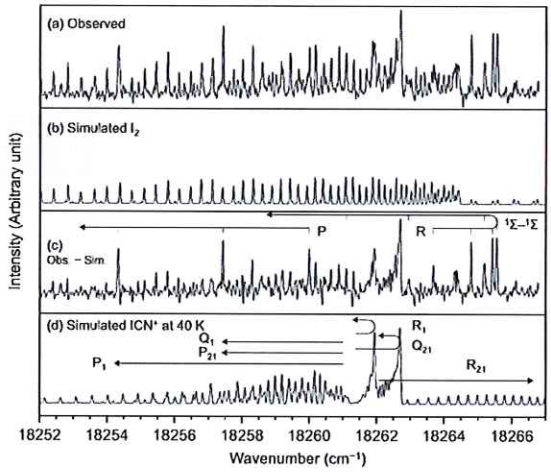

Fig. 1. The electronic spectrum of the $\widetilde{A}\ ^2\Sigma^+$–$\widetilde{X}\ ^2\Pi_{3/2}$ transition of ICN^+. (a) Uncorrected cavity ring-down spectrum observed in a pulsed supersonic slit jet expansion of ICN. (b) Simulated spectrum of the sub-product iodine molecules, I_2, using the reported molecular constants and FC factors [21,22]. (c) Subtraction of (b) from (a) giving a spectrum free from iodine molecules. (d) Simulated spectrum of ICN^+ using the molecular parameters determined in the present experiment.

parameter for the other cations can be estimated with the aid of theoretical calculation.

In the present work, a rotationally resolved high-resolution optical absorption spectrum of the $\widetilde{A}\ ^2\Sigma^+$–$\widetilde{X}\ ^2\Pi_{3/2}$ electronic transition of ICN^+ was observed for the first time by cavity ring-down spectroscopy. In addition, we calculated the rotational constants for four analogous cations (FCN^+, $ClCN^+$, $BrCN^+$, and ICN^+) in order to argue the temperature dependence of the rotational structure in the $\widetilde{A}\ ^2\Sigma^+$–$\widetilde{X}\ ^2\Pi_{3/2}$ electronic transition. Finally, an astrophysical feature of $ClCN^+$, one of the candidates for DIB carriers, will be discussed.

2. Methods

Cavity ring-down spectroscopy is a powerful way to sensitively measure pure-absorption spectra of gas-phase molecules by using a cavity constructed with a couple of highly reflective mirrors ($R \sim 99.99\%$). The experimental apparatus in this work consisted of a standard cavity ring-down setup sampling a plasma generated in a pulsed supersonic slit jet expansion [18,19]. A spectrum was recorded by measuring ring-down times as a function of the wavelength of the dye laser pumped by the excimer laser running at 30 Hz. The spectrum was scanned with a step of 0.013 cm^{-1}, where forty-five ring-down events were averaged at each wavelength. The 0.05-cm^{-1} linewidth of the laser was attained with an intracavity étalon.

The pulsed slit jet system was located in a vacuum chamber evacuated by a roots blower pump [20]. The plasma was produced in a nozzle incorporating a discharge in the high-pressure super-sonic expansion. The orifice comprised a metal plate anode and two sharp stainless-steel cathodes that formed the actual slit of 30 mm × 300 μm. A pulsed negative voltage of −800 V was applied 100 ms in duration. The discharge is thought to be confined upstream of the supersonic expansion due to the geometry of the orifice. To produce ICN^+, solid ICN was heated in an oven to 50 °C, and then evaporated component was mixed with helium as a carrier gas at a backing pressure of 10 bars. ICN^+ was efficiently produced at a distance of ~5 mm downstream from the slit. The spectrum was calibrated *via* the $B\ ^3\Pi(0_u^+)$–$X\ ^1\Sigma_g^+$ absorption lines of iodine molecules that were simultaneously observed in the same jet expansion [21,22].

To derive the rotational constants for the four cyanogen halide radical cations (FCN^+, $ClCN^+$, $BrCN^+$, ICN^+), we calculated their structures by CAM-B3LYP/CEP-121G using the program package Gaussian 09W [23].

Table 1
Observed rotational electronic transitions of the $\widetilde{A}\ ^2\Sigma^+$–$\widetilde{X}\ ^2\Pi_{3/2}$ transition for ICN^+.

	J'		J''	ν_{obs} (cm^{-1})	$\nu_{obs} - \nu_{cal}$ (cm^{-1})
R_{21}	8.5	–	7.5	18264.135	−0.001
	10.5	–	9.5	18264.704	−0.007
	11.5	–	10.5	18264.987	−0.001
	12.5	–	11.5	18265.256	−0.005
	14.5	–	13.5	18265.794	0.008
	15.5	–	14.5	18266.042	0.001
	16.5	–	15.5	18266.291	0.002
	17.5	–	16.5	18266.536	0.005
	18.5	–	17.5	18266.762	−0.005
Q_{21}	6.5	–	6.5	18262.103	−0.006
	7.5	–	7.5	18262.191	−0.001
	8.5	–	8.5	18262.270	0.002
	9.5	–	9.5	18262.336	−0.003
	10.5	–	10.5	18262.398	−0.005
	11.5	–	11.5	18262.462	−0.000
	12.5	–	12.5	18262.506	−0.008
	13.5	–	13.5	18262.557	−0.003
P_1	20.5	–	21.5	18252.627	0.002
	19.5	–	20.5	18253.085	−0.010
	18.5	–	19.5	18253.562	0.001
	14.5	–	15.5	18255.371	0.010
	11.5	–	12.5	18256.646	−0.001
	9.5	–	10.5	18257.477	0.001

3. Results and discussion

3.1. Assignment of rotational lines

The absorption spectrum for the 0–0 band of the $\widetilde{A}\ ^2\Sigma^+$–$\widetilde{X}\ ^2\Pi_{3/2}$ electronic transition of ICN^+ was recorded in the 18252–18267 cm^{-1} region, as shown in Fig. 1a. However, many sharp lines from iodine molecules, which were also produced from ICN in discharge, were overlapped. We used *a program for rotational, vibrational and electronic spectra* PGOPHER [24] to simulate the iodine-molecule spectrum from the reported molecular constants and FC factors [21,22], as described in Fig. 1b. The rotational temperature of 30 K and the vibrational temperature of 400 K were assumed in the simulation. Subtraction of Fig. 1b from Fig. 1a gives a spectrum free from iodine molecules as shown in Fig. 1c. This spectral trace is contributed from two different absorption bands; one is the $\widetilde{A}\ ^2\Sigma^+(v' = 0)$–$\widetilde{X}\ ^2\Pi_{3/2}(v'' = 0)$ electronic transition of ICN^+. Another consists of 11 strong lines marked by P and R branches definitely belonging to the $^1\Sigma$–$^1\Sigma$ transition of a molecule or an ion. The transition wavenumbers of this unknown species are listed in Appendix (Table A1). From the numerical analysis, the rotational constants of the ground and excited states are determined to be 1.04734(83) and 0.80159(69) cm^{-1}, respectively, and the band origin to be 18262.083(3) cm^{-1}, where the values in parentheses denote the uncertainties and apply to the last digit of the values. Though it is clear that the carrier involves no iodine atoms due to the large rotational constants, we could not find any suitable candidate in the past literature. The possibility that this band is corresponding to the transition between electronically excited vibronic levels will not be ruled out.

The ground-state rotational constant of ICN^+ was reported to be 0.1107 cm^{-1} from FC analysis of the photoelectron spectra [17]. We used this value as an initial parameter to get the entire picture of the rotational structure as shown in Fig. 1d. Subsequently, the transition wavenumbers corresponding to the R_{21}, Q_{21}, and P_1 branches listed in Table 1 were used to determine molecular constants. This is because the three branches show less overlapping with other lines, while the peaks of

Table 2
Determined molecular constants of ICN^+.

State	Constants	Values (cm^{-1})[a]
$\tilde{X}^2\Pi_{3/2}$	B''	0.11002(12)
$\tilde{A}^2\Sigma^+$	T_0	18261.2319(30)
	B'	0.10700(12)
	γ	−0.04100(69)

[a] Values in parentheses denote the uncertainties (1σ) and apply to the last digit of the values.

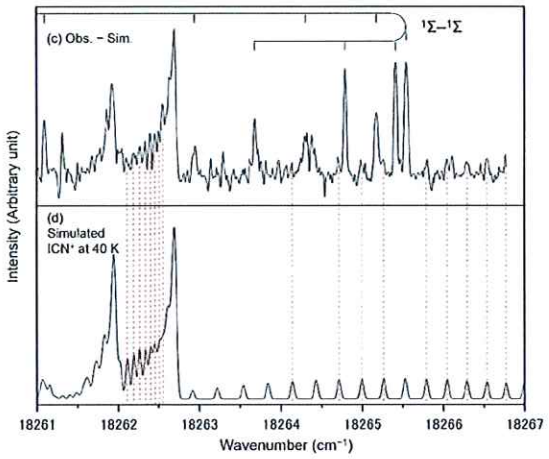

Fig. 2. Expanded spectra of Fig. 1c and d in the region around R_1-, Q_{21}-, and R_{21}-branches. The spectral lines indicated by the red dotted lines were used for the determination of molecular parameters (see Table 1).

the R_1, P_{21}, and Q_1 branches are difficult to be picked up due to heavy overlapping. We could find the set of the rotational constants of both the $\tilde{A}\,^2\Sigma^+(v' = 0)$ and $\tilde{X}\,^2\Pi_{3/2}(v'' = 0)$ states, the band-origin position T_0, and the splitting constant γ of the upper state by line-position fitting with PGOPHER, as listed in Table 2. Especially the rotational constants were precisely determined through the rotational structure and the ground-state rotational constant agrees with the reported value [17] within 1%. The simulated spectrum at 40 K using these parameters reproduces well the measured rotational structure including the band heads of the R_1 and Q_{21} branches at 18262.0 and 18262.7 cm^{-1}, respectively, as shown in Fig. 2.

3.2. Rotational constant ratios of the halogen cyanide radical cations

The ratio β for rotational constants defined as $\beta = (B' - B'')/B''$ can be a simple measure for the degree of change of the rotational constants in the upper and lower states. The value of β would be useful for arguing the spectral variation by temperature change as mentioned in the following section. For ICN^+, the value of β was experimentally determined to be −2.8% in the present study, showing that the rotational constant of the $\tilde{A}\,^2\Sigma^+$ ($v' = 0$) is smaller than that of $\tilde{X}\,^2\Pi_{3/2}$ ($v'' = 0$). For the analogous cyanide cations, FCN^+, $ClCN^+$, and $BrCN^+$, the values of β have not been experimentally determined by rotational analysis. To estimate β for these species, the optimized structures of the $\tilde{A}\,^2\Sigma^+$ and $\tilde{X}\,^2\Pi_{3/2}$ states were calculated by CAM-B3LYP/CEP-121G using Gaussian 09 W. The calculations gave the anti-symmetric stretching vibration frequencies of 2026, 1904, 1900, and 1984 cm^{-1} in the $\tilde{X}\,^2\Pi_{3/2}$ state for FCN^+, $ClCN^+$, $BrCN^+$, and ICN^+, which agree well with the observed values of ~2100 [25], 1916, 1906, and 2082 cm^{-1} [9], respectively. This fact ensures the accuracy of our calculations. The obtained β values are listed in Table 3. It was found that the calculated β, as shown by the black squares in Fig. 3, decreases along with the increase of the size of the halogen atom. The ratios for FCN^+ and $ClCN^+$ derived from the reported rotational constants by FC calculation [10], represented by red open circles, are close to the calculated β values. The calculated β value for ICN^+ agrees reasonably with that (the red filled circle) determined by rotational analysis in the current work within an accuracy of the calculations.

Table 3
Ground-state rotational constants and rotational-constant ratios of the cyanogen halide radical cations.

	Calculated[a]		Estimated[b]		Observed[c]	
	β	B'' ($\tilde{X}^2\Pi_{3/2}$) (cm^{-1})	β	B'' ($\tilde{X}^2\Pi_{3/2}$) (cm^{-1})	β	B'' ($\tilde{X}^2\Pi_{3/2}$) (cm^{-1})
FCN^+	6.7	0.331	6.2	0.353		
$ClCN^+$	1.6	0.190	1.5	0.205		
$BrCN^+$	0.0	0.135				
ICN^+	−1.3	0.108			−2.8	0.110

[a] This work; values calculated by CAM-B3LYP/CEP-121G.
[b] FC calculation by Ref. [10].
[c] This work; values obtained by rotational analyses.

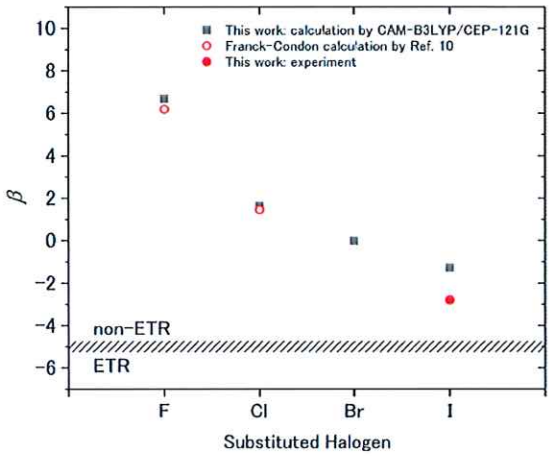

Fig. 3. Rotational constant ratios β of the four species of the cyanogen halide radical cations XCN^+. The value of $\beta \sim -5$ is considered to be a rough borderline between non-ETR and ETR for a rotational profile of an electronic transition in a diffuse cloud [27].

3.3. Astrophysical relevance

Although ICN^+ is an unlikely candidate of DIB, $ClCN^+$ can be a good candidate of DIB because of the abundance of the chlorine element in space. Additionally, a large quantity of chlorides has been detected in interstellar clouds so far [26]. DIBs can be classified into two categories by whether their profiles depend on temperature or not. The first group is denoted as ETR (abbreviation of an extended tail toward red) in which the spectral contour becomes gradually weaker and weaker toward longer wavelength when a temperature of a diffuse cloud is high [27]. Another can be designated as non-ETR in which the spectral contour exhibits a symmetric profile irrespective of temperature; it is considered that a DIB shows non-ETR behavior for $|\beta| < 5\%$ and ETR behavior for $\beta < -5\%$. According to this standard as indicated in Fig. 3, the three cations, $ClCN^+$, $BrCN^+$, and ICN^+, can show non-ETR behavior.

Finally, we would like to discuss how the spectral profile of the $\tilde{A}\,^2\Sigma^+$–$\tilde{X}\,^2\Pi_{3/2}$ transition of $ClCN^+$ varies with temperature. Fulara et al. [9] reported the peak positions of the 0–0 bands of the $\tilde{A}\,^2\Sigma^+$–$\tilde{X}\,^2\Pi_{3/2}$ transition of $ClCN^+$ to be 11689 ± 1 and 11691 ± 1 cm^{-1} (indicated by red dotted lines in Fig. 4a) for the ^{35}Cl and ^{37}Cl isotopologues,

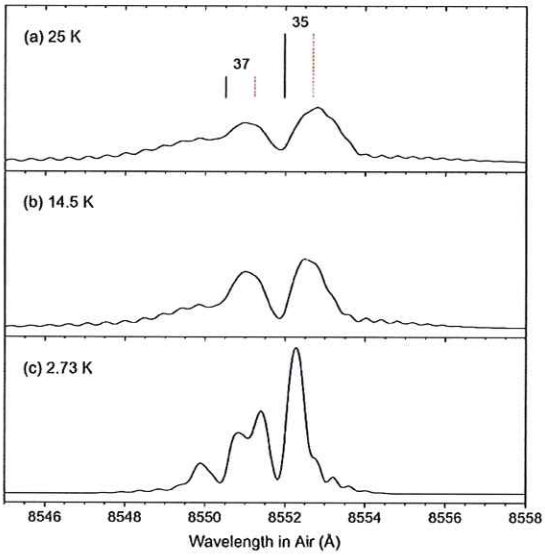

Fig. 4. The variation of the $\tilde{A}\,^2\Sigma^+$–$\tilde{X}\,^2\Pi_{3/2}$ transition of $ClCN^+$ at three different ambient temperatures. Red dotted lines; reported peak positions of the two isotopologues in the emission spectra [9]. Black solid lines; band-origin positions assumed for reproducing that the simulated peak maxima meet with red dotted lines. The abundance ratio; ^{35}Cl:$^{37}Cl = 3:1$, the rotational constant ratio; $\beta = 1.6$, the splitting constant; $\gamma = 0$. Due to the experimental error of [9], an uncertainty of ±0.3 Å needs to be considered.

respectively, *via* the rotationally cooled emission spectrum. The accuracy of the peak positions (±1 $cm^{-1} \approx \pm 0.3$ Å) is narrower than a typical bandwidth of DIB (~1 Å), although this value is less accurate than that determined by a telescope (0.1–0.3 Å, e.g. [28]), allowing us to attempt a preliminary identification of DIBs. The black trace in Fig. 4a shows the simulated rotational contour at 25 K. To reproduce the results by Fulara et al., the band origins of the two isotopologues of $ClCN^+$ were assumed to be at 11,690 and 11,692 cm^{-1} (indicated by black solid lines) for ^{35}Cl and ^{37}Cl, respectively. Additionally, it was assumed that the abundance ratio of the isotopologues is ^{35}Cl:$^{37}Cl = 3:1$, the rotational constants ratio is $\beta = 1.6$ (Calculated, Table 3), and the splitting constant of the $\tilde{A}\,^2\Sigma^+$ state is $\gamma = 0$ [29]. The resolution of a spectrum was set at 0.3 Å. The stronger peak at 8552.8 Å (11689 cm^{-1}) is produced by a blending of the P- and Q-branches of the ^{35}Cl isotopologue, and the weaker peak at 8551.0 Å (11691 cm^{-1}) is by the R-branch of ^{35}Cl and the P- and Q-branches of ^{37}Cl. The observed β value of ICN^+ is slightly smaller than the calculated value (Fig. 3). On the other side, due to the smaller β value than 1.6 for $ClCN^+$, the location and profile of these peaks don't change much in temperature of ≤25 K. The simulated rotational profiles at 14.5 and 2.73 K [27] are shown in Fig. 4b and c, respectively. In the case of 14.5 K, the interval between two broad peaks appearing at 8552.6 and 8551.1 Å becomes narrower than at 25 K. In the case of 2.73 K, the spectral profile changes considerably; the peak width becomes much sharper and the interval between peaks becomes even narrower. For all cases at 2.73–25 K, the peaks do not include the band-head components of individual branches and do not show ETR because of the small $|\beta|$. Rather this transition would show the extended tail toward "blue" because the ^{37}Cl isotopologue makes a shoulder at a blue side of the profile. These profiles may allow us to identify the absorption band of $ClCN^+$ in space. At present, a related peak is not listed in the survey catalog for the stars HD183143 and HD204827 [28]. Further near-infrared surveys are greatly anticipated.

4. Summary and conclusions

The gas-phase rotationally resolved spectrum of the $\tilde{A}\,^2\Sigma^+$–$\tilde{X}\,^2\Pi_{3/2}$ electronic transition of ICN^+ around 548 nm was recorded in the discharge jet by cavity ring-down spectroscopy. After removing the contaminating iodine-molecule lines, the rotational structure of ICN^+ appeared clearly. The rotational constants, the splitting constant, and the band origin were derived through the assignment of the rotational lines by the line-position fitting. The observed rotational structure including the two band heads of the R_1 and Q_{21} blanches were well reproduced by the simulation at the rotational temperature of 40 K. The obtained rotational constants show the small rotational constant ratio ($\beta_{obs} = -2.8\%$), which agrees reasonably with the theoretically calculated ratio ($\beta_{calc} = -1.3\%$). The β values for FCN^+, $ClCN^+$, and $BrCN^+$ were also evaluated theoretically. The rotational profile of the absorption band and its temperature dependence for $ClCN^+$, one of the important candidates for DIBs, were estimated, allowing us the identification of this cation as in space.

CRediT authorship contribution statement

Mitsunori Araki: Conceptualization, Investigation, Validation, Writing – original draft. **Takumi Ito:** Investigation, Formal analysis. **Shoma Hoshino:** Writing – review & editing. **Koichi Tsukiyama:** Writing – review & editing, Supervision.

Declaration of Competing Interest

The authors declare that they have no known competing financial interests or personal relationships that could have appeared to influence the work reported in this paper.

Acknowledgments

The spectroscopic data were obtained during M.A.'s stay at the University of Basel in the group of Prof. J.P. Maier. M.A. thanks Grant-in-Aid for Scientific Research (C) (Grant No. 18K05045) and for Challenging Research (Exploratory) (Grant No. 21K18663), Paloma environmental technology development foundation, Yamada Science Foundation, ESPEC Foundation for Global Environment Research and Technology, Yashima Environment Technology Foundation, and Takahashi Industrial and Economic Research Foundation.

Appendix

Table A1.

Table A1
Observed rovibronic transitions of the $^1\Sigma$–$^1\Sigma$ transition for unknown species.

	J'		J''	ν_{obs} (cm^{-1})	$\nu_{obs} - \nu_{cal}$ (cm^{-1})
R(J)	1	–	0	18263.683	−0.003
	2	–	1	18264.791	−0.006
	3	–	2	18265.414	−0.001
	4	–	3	18265.543	0.003
	5	–	4	18265.176	0.005
	6	–	5	18264.307	−0.001
	7	–	6	18262.946	−0.004
	8	–	7	18261.100	0.002
P(J)	0	–	1	18259.999	0.010
	2	–	3	18254.324	−0.004
	3	–	4	18250.762	−0.003
	4	–	5	18246.715	0.002

Note. The spectral analysis results in the rotational constants of 1.04734(83) and 0.80159(69) cm^{-1}, the centrifugal distortion constants of 3.3(22) and 2.9(14) × 10^{-5} cm^{-1} in the lower and upper states, respectively, and the band origin of 18262.083(3) cm^{-1}. The values in parentheses denote the uncertainties (1σ) and apply to the last digit of the values.

References

[1] G.H. Herbig, The diffuse interstellar bands, Annu. Rev. Astron. Astrophys. 33 (1) (1995) 19–73.

[2] J. Cami, N.L.J. Cox, The diffuse interstellar bands, in: Proc. Int. Astron. Union, IAU Symp., Cambridge University Press, Noordwijkerhout, The Netherlands, 2014.

[3] M.L. Heger, Further study of the sodium lines in class B stars, Lick Obs. Bull. 10 (1922) 141–145, https://doi.org/10.5479/ADS/bib/1922LicOB.10.141H.

[4] B.J. McCall, R.E. Griffin, On the discovery of the diffuse interstellar, bands 469 (2013), https://doi.org/10.1098/rspa.2012.0604.

[5] E.K. Campbell, M. Holz, D. Gerlich, J.P. Maier, Laboratory confirmation of C_{60}^+ as the carrier of two diffuse interstellar bands, Nature 523 (7560) (2015) 322–323, https://doi.org/10.1038/nature14566.

[6] G.A.H. Walker, D.A. Bohlender, J.P. Maier, E.K. Campbell, Identification of more interstellar C_{60}^+ bands, Astrophys. J. 812 (2015) L8, https://doi.org/10.1088/2041-8205/812/1/L8.

[7] E.K. Campbell, M. Holz, J.P. Maier, D. Gerlich, G.A.H. Walker, D. Bohlender, Gas phase absorption spectroscopy of C_{60}^+ and C_{70}^+ in a cryogenic ion trap: comparison with astronomical measurements, Astrophys. J. 822 (2016) 17, https://doi.org/10.3847/0004-637X/822/1/17.

[8] E.K. Campbell, M. Holz, J.P. Maier, C_{60}^+ in diffuse clouds: laboratory and astronomical comparison, Astrophys. J. 826 (2016) L4, https://doi.org/10.3847/2041-8205/826/1/L4.

[9] J. Fulara, D. Klapstein, R. Kuhn, J.P. Maier, Emission spectra of supersonically cooled halocyanide cations, XCN^+ (X = Cl, Br, I): $\tilde{A}^2\Sigma^+ \rightarrow X^2\Pi$ and $\tilde{B}^2\Pi \rightarrow X^2\Pi$ band systems, J. Phys. Chem. 89 (1985) 4213–4219, https://doi.org/10.1021/j100266a014.

[10] D.-C. Wang, F.-T. Chau, E. Lee, A. Leung, J. Dyke, The $X^2\Pi$ and $A^2\Sigma$ states of FCN^+ and $ClCN^+$: ab initio calculations and simulation of the He I photoelectron spectra of FCN and ClCN, Mol. Phys. 93 (6) (1998) 995–1005, https://doi.org/10.1080/00268979809482286.

[11] J.M. Hollas, T.A. Sutherley, Geometry of cyanogen halide positive ions from photoelectron spectroscopy, Mol. Phys. 22 (1971) 213–223, https://doi.org/10.1080/00268977100102491.

[12] B. Kovač, High-resolution photoelectron spectra of BrCN and ICN: Vibronic mixing, J. Phys. Chem. 91 (1987) 4231–4235, https://doi.org/10.1021/j100300a005.

[13] J.H.D. Eland, P. Baltzer, L. Karlsson, B. Wannberg, The photoelectron spectrum of iodine cyanide, ICN, Chem. Phys. 222 (1997) 229–240, https://doi.org/10.1016/S0301-0104(97)00214-0.

[14] M. Allan, E. Heilbronner, E. Kloster-Jensen, J.P. Maier, The $\prod$-states of tetraacetylene radical cation, Chem. Phys. Lett. 41 (1976) 228–230, https://doi.org/10.1016/0009-2614(76)80798-1.

[15] M. Tsuji, J.P. Maier, Emission spectra of $N_2O^+(A^2\Sigma^+\text{-}X^2\Pi)$, $CS_2^+(A^2\Pi_u\text{-}X\ ^2\Pi_g)$ and $ICN^+(A^2\Sigma^+\text{-}X^2\Pi)$ excited by penning ionization in low-pressure neon and helium afterglows, Chem. Phys. 126 (1988) 435–440, https://doi.org/10.1016/0301-0104(88)85051-1.

[16] S. Leutwyler, J.P. Maier, U. Spittel, The electronic absorption spectra of $ClCN^+$, $BrCN^+$, and ICN^+ in neon matrices, J. Chem. Phys. 83 (1985) 506–510, https://doi.org/10.1063/1.449513.

[17] F.T. Chau, C.A. McDowell, Y.W. Tang, Determination of geometries and molecular properties of XCN^+ ions (where X is Cl, Br, I) through Franck-Condon analyses on the corresponding photoelectron spectra, J. Electron Spectros. Relat. Phenomena. 61 (1993) 217–229, https://doi.org/10.1016/0368-2048(93)80052-N.

[18] T. Motylewski, H. Linnartz, Cavity ring down spectroscopy on radicals in a supersonic slit nozzle discharge, Rev. Sci. Instrum. 70 (1999) 1305–1312, https://doi.org/10.1063/1.1149589.

[19] H. Linnartz, T. Motylewski, J.P. Maier, The $^2\Pi \leftarrow X^2\Pi$ electronic spectra of C_8H and $C_{10}H$ in the gas phase, J. Chem. Phys. 109 (1998) 3819–3823, https://doi.org/10.1063/1.476981.

[20] P. Cias, M. Araki, A. Denisov, J.P. Maier, Gas phase detection of cyclic B_3: $2^2E' \leftarrow X^2A'_1$ electronic origin band, J. Chem. Phys. 121 (2004) 6776–6778, https://doi.org/10.1063/1.1791153.

[21] P. Luc, Molecular constants and Dunham expansion parameters describing the B-X system of the iodine molecule, J. Mol. Spectrosc. 80 (1980) 41–55, https://doi.org/10.1016/0022-2852(80)90269-6.

[22] F. Martin, R. Bacis, S. Churassy, J. Vergès, Laser-induced-fluorescence Fourier transform spectrometry of the XO_g^+ state of I_2: Extensive analysis of the $BO_u^+ \rightarrow XO_g^+$ fluorescence spectrum of $^{127}I_2$, J. Mol. Spectrosc. 116 (1986) 71–100, https://doi.org/10.1016/0022-2852(86)90254-7.

[23] M.J. Frisch, G.W. Trucks, H.B. Schlegel, G.E. Scuseria, M.A. Robb, J.R. Cheeseman, G. Scalmani, V. Barone, G.A. Petersson, H. Nakatsuji, X. Li, M. Caricato, A. Marenich, J. Bloino, B.G. Janesko, R. Gomperts, B. Mennucci, H.P. Hratchian, J. V. Ortiz, A.F. Izmaylov, J.L. Sonnenberg, D. Williams-Young, F. Ding, F. Lipparini, F. Egidi, J. Goings, B. Peng, A. Petrone, T. Henderson, D. Ranasinghe, V. G. Zakrzewski, J. Gao, N. Rega, G. Zheng, W. Liang, M. Hada, M. Ehara, K. Toyota, R. Fukuda, J. Hasegawa, M. Ishida, T. Nakajima, Y. Honda, O. Kitao, H. Nakai, T. Vreven, K. Throssell, J.A.J. Montgomery, J.E. Peralta, F. Ogliaro, M. Bearpark, J. J. Heyd, E. Brothers, K.N. Kudin, V.N. Staroverov, T. Keith, R. Kobayashi, J. Normand, K. Raghavachari, A. Rendell, J.C. Burant, S.S. Iyengar, J. Tomasi, M. Cossi, J.M. Millam, M. Klene, C. Adamo, R. Cammi, J.W. Ochterski, R.L. Martin, K. Morokuma, O. Farkas, J.B. Foresman, D.J. Fox, Gaussian 09, Revision A.02 (2016). https://gaussian.com/g09citation/.

[24] C.M. Western, PGOPHER, A Program for Simulating Rotational, Vibrational and Electronic Spectra, University of Bristol, (n.d.).

[25] G. Bieri, Cyanogen fluoride: a photoelectron-spectroscopic investigation, Chem. Phys. Lett. 46 (1977) 107–110, https://doi.org/10.1016/0009-2614(77)85173-7.

[26] B.A. McGuire, 2021 census of interstellar, circumstellar, extragalactic, protoplanetary disk, and exoplanetary molecules, Astrophys. J. Suppl. Ser. 259 (2022) 30, https://doi.org/10.3847/1538-4365/ac2a48.

[27] T. Oka, D.E. Welty, S. Johnson, D.G. York, J. Dahlstrom, L.M. Hobbs, Anomalous diffuse interstellar bands in the spectrum of herschel 36. II. Analysis of radiatively excited CH^+, CH, and diffuse interstellar bands, Astrophys. J. 773 (2013) 42, https://doi.org/10.1088/0004-637X/773/1/42.

[28] H. Fan, L.M. Hobbs, J.A. Dahlstrom, D.E. Welty, D.G. York, B. Rachford, T.P. Snow, P. Sonnentrucker, N. Baskes, G. Zhao, The apache point observatory catalog of optical diffuse interstellar bands, Astrophys. J. 878 (2019) 151, https://doi.org/10.3847/1538-4357/ab1b74.

[29] M.A. King, R. Kuhn, J.P. Maier, $A^2\Sigma^+ \rightarrow X^2\Pi_i$ emission spectra of the supersonically cooled cations HCP^+ and DCP^+, Mol. Phys. 60 (1987) 867–879, https://doi.org/10.1080/00268978700100581.